JOURNAL OF Materials CHEMISTRY

Synthesis, structure and lithium-ion conductivity of $Li_{2-2x}Mg_{2+x}(MoO_4)_3$ and $Li_3M(MoO_4)_3$ (M^{III} = Cr, Fe)†

Litty Sebastian,[a] Y. Piffard,[b] A. K. Shukla,[a] F. Taulelle[c] and J. Gopalakrishnan*[a]

[a]*Solid State and Structural Chemistry Unit, Indian Institute of Science, Bangalore 560 012, India*
[b]*Institut des Matériaux Jean Rouxel, UMR CNRS-Université de Nantes n° 6502, 2, rue de la Houssinière, BP 32229, 44322 Nantes Cedex 03, France*
[c]*RMN et Chimie du Solide, Tectonique Moléculaire du Solide UMR 7140 CNRS, Université Louis Pasteur, 4, Rue Blaise Pascal, 67070 Strasbourg, France*

Received 3rd February 2003, Accepted 16th May 2003
First published as an Advance Article on the web 3rd June 2003

Lithium magnesium molybdates of the general formula $Li_{2-2x}Mg_{2+x}(MoO_4)_3$, for $0 \leqslant x \leqslant 0.3$, have been synthesized and their structure and lithium ion conductivity investigated. Determination of crystal structure of one of the members, $Li_2Mg_2(MoO_4)_3$, has revealed a three-dimensional framework consisting of metal–oxygen octahedra and trigonal prisms (where Li and Mg reside) which are interconnected by MoO_4 tetrahedra. Although the framework is three-dimensional, lithium-ion conductivity appears to be restricted to the one-dimensional channels formed by interconnected trigonal prisms. Isotypic molybdates, $Li_3M(MoO_4)_3$ (M = Cr, Fe), where lithium ions occupy exclusively the trigonal prismatic channels, exhibit a higher lithium ion conductivity than $Li_{2-2x}Mg_{2+x}(MoO_4)_3$, lending support to the idea that the conductivity is one-dimensional in these materials. ^{7}Li NMR spectral data are consistent with this interpretation.

Introduction

Metal oxides containing mobile lithium ions are important materials as electrodes and electrolytes for lithium batteries.[1,2] The mobility of the lithium ion in solids manifests itself in the following measureable properties: ionic conductivity/diffusion, redox insertion/deinsertion and ion exchange. While insertion/deinsertion of lithium under electrochemical redox conditions determines the practical use of a solid as an electrode,[3] a high lithium ion conductivity is important for the development of electrolyte materials for lithium batteries.[4] A high mobility of lithium occurs both in anion close packed metal oxides (*e.g.* $LiCoO_2$ and $LiMn_2O_4$ spinels) as well as in open framework oxides. NASICON ($Na_3Zr_2PSi_2O_{12}$) is a well-known example of the latter,[5] whose framework, consisting of interconnected metal–oxygen octahedra and tetrahedra, is known to support a high mobility for lithium giving rise to fast lithium ion conduction (*e.g.* $Li_{1+x}Ti_{2-x}Al_x(PO_4)_3$ and $LiTaAl(PO_4)_3$)[6,7] as well as redox insertion/extraction of lithium (*e.g.* $Li_2NaV_2(PO_4)_3$).[8]

In a search for other framework oxides with high lithium ion mobility, we recently synthesized $LiMgFSO_4$, a new sphene ($CaTiOSiO_4$) derivative, that exhibits significant lithium ion conduction.[9] In our attempts to synthesize the molybdate analog of this material, we obtained another framework oxide of the formula $Li_{2-2x}Mg_{2+x}(MoO_4)_3$, belonging to the $Li_2M_2(MoO_4)_3$ (M^{II} = Mn, Fe, Co, Ni) family.[10–13] Considering that the structure of the latter series consists of interconnected octahedra, tetrahedra and trigonal prisms that would provide pathways for lithium ion mobility, we synthesized and investigated the structure and ionic conductivity of members of the series $Li_{2-2x}Mg_{2+x}(MoO_4)_3$ as well as the related $Li_3M^{III}(MoO_4)_3$ for M^{III} = Cr, Fe. We also determined the detailed crystal structure of one of the members, $Li_2Mg_2(MoO_4)_3$, in an attempt to understand the relation between structure and lithium ion conductivity. The results, which are described herein, suggest that although the framework of these oxides is three-dimensional, lithium ion conductivity appears to be restricted to one-dimensional channels (along the *a*-direction of the orthorhombic structure) that contain lithium in trigonal prismatic coordination.

Experimental

Oxides of the series $Li_{2-2x}Mg_{2+x}(MoO_4)_3$ were synthesized by reacting Li_2CO_3, MgO and MoO_3 in stoichiometric proportions for different values of x in the temperature range 575–650 °C for various times in air. Similarly, $Li_3M(MoO_4)_3$ (M = Cr, Fe) were prepared from the constituent oxides around 600 °C in air. Formation of single-phase products was investigated by powder X-ray diffraction (Siemens D5005 X-ray Diffractometer, CuK_α). Single crystals of $Li_2Mg_2(MoO_4)_3$ were obtained from a mixture of Li_2CO_3, MgO, MoO_3 and NH_4F, with a 10% excess (by weight) of Li_2CO_3 and NH_4F, taken in a Pt crucible and reacted at 750 °C for 18 hours and cooled to room temperature slowly. They crystallize as rather thick colorless needles of sufficient size for crystallographic study; the composition of the crystals was determined by atomic microprobe analysis on a scanning electron microscope and flame photometry.

Preliminary cell parameters were inferred from 25 reflections obtained from an automatically centered crystal on a CAD4 Enraf-Nonius diffractometer. They were further refined from the powder diffraction pattern recorded in Debye–Scherrer geometry using an INEL CPS 120 diffractometer equipped with a quartz monochromator ($CuK_{\alpha1}$, λ = 1.540598 Å). The refinement was done with the full pattern matching procedure using the program FULLPROF[14] and the cell parameters are given in Table 1.

Single-crystal intensity data were collected, at room temperature, under the conditions given in Table 1. Data reduction was carried out with the use of programs in the SHEXTL Plus package[15] and the structure was refined using

†Electronic supplementary information (ESI) available: anisotropic displacement parameters and XRPD data for $Li_2Mg_2(MoO_4)_3$. See http://www.rsc.org/suppdata/jm/b3/b301189e/

Table 1 Crystallographic data for $Li_2Mg_2(MoO_4)_3$

Formula	$Li_2Mg_2(MoO_4)_3$
Formula mass	539.3
Space group	*Pnma*
a/Å	5.1167(2)
b/Å	10.4646(4)
c/Å	17.6228(8)
V/Å^3	943.59(7)
Z	4
ρ_c/g cm^{-3}	3.798
μ(MoKα)/cm^{-1}	41.2
Crystal dimensions/mm	0.17 × 0.045 × 0.045
Scan mode	θ–2θ
θ limits/°	2.0–40.0
Data collected	$-1 \leqslant h \leqslant 8$, $-1 \leqslant k \leqslant 18$, $-1 \leqslant l \leqslant 30$
No. of reflections (n) with $I > 3\sigma(I)$ (observed)	1740
Number of variables (p)	86
$R(F)$[a] (for obs. reflections)	0.0308
$R_w(F)$[b] (for obs. reflections)	0.0240
$S^c = [\Sigma\,[w(F_o - F_c)^2]/(n-p)]^{1/2}$	1.70
$\Delta\rho_{max}$; $\Delta\rho_{min}$/e$^-$ Å^{-3}	2.6; −2.35

[a] $R(F) = \Sigma||F_o| - |F_c||/\Sigma|F_o|$. [b] $R_w(F) = [\Sigma w(|F_o| - |F_c|)^2/\Sigma w F_o^2]^{1/2}$ with $w = 1/[\sigma^2(F_o)]$. [c] Calculated with all reflections (2645).

the JANA98 program package.[16] Conventional atomic scattering factors and anomalous dispersion corrections[17] were used. An absorption correction was not deemed necessary. Atomic positions of $Li_2Co_2(MoO_4)_3$[13] were used as the initial input for the refinement. The structure was then refined by the least-squares method, involving anisotropic displacement parameters for Mo and O atoms and the distribution of Li/Mg atoms over the three M sites (considered as fully occupied and with the constraint that the sums of Li and Mg occupancies are equal in order to fulfil the stoichiometry).

CCDC reference number 207253. See http://www.rsc.org/suppdata/jm/b3/b301189e/ for crystallographic data in CIF or other electronic format.

^{7}Li NMR spectra were acquired on a DSX 500 Bruker spectrometer equipped with a 4 mm MAS probe head from Bruker. The ^{7}Li resonating frequency was 194.32 MHz and all chemical shifts are referenced to a LiCl solid sample (or saturated solution in water). Sample were spun at about 10 kHz, and large spectral excitation conditions, in single pulse mode, were used with small pulse length (usually 1 μs) and large RF field (~100 kHz). Analysis of spectra was carried out with Winfit software.[18]

Lithium ion conductivities were measured on sintered pellets coated with gold paste (cured at 600 °C for 6 h) using a HP4194A Impedance/Gain-Phase Analyzer over the frequency range 100 Hz–15 MHz in the temperature range 30–600 °C in air. For each sample, measurement was made for both heating and cooling cycles. Samples were equilibrated at constant temperature for about 1 hour prior to each impedance measurement.

Results and discussion

Reaction of Li_2CO_3, MgO and MoO_3 in the solid state around 575–600 °C yielded a new molybdate different from Li_2MoO_4 and $MgMoO_4$. We could grow single crystals of the new molybdate from the constituents, as described in the Experimental section. The atomic microprobe analysis of single crystals of the new molybdate showed the Mg:Mo ratio to be 2:3. Independent lithium analysis using flame photometry showed the presence of two lithium atoms per formula unit corresponding to the formula $Li_2Mg_2(MoO_4)_3$.

We determined the crystal structure of the molybdate from single crystal X-ray diffraction data. The final cycle of refinement of the structure of $Li_2Mg_2(MoO_4)_3$ resulted in residuals of $R = 0.0308$ and $R_w = 0.0240$. Final values of positional parameters are given in Table 2. A list of selected bond distances and bond valence sums[19,20] is given in Table 3. The interplanar distances and intensities calculated from the structure using the program POWDERCELL[21] are in agreement with the observed interplanar spacings and intensities. These data will be deposited with ICDD.

The crystal structure (Fig. 1) is essentially the same as that of $Li_2Co_2(MoO_4)_3$[13] and other similar divalent metal molybdates,[10–12] consisting of five different coordination polyhedra: two of them are crystallographically independent MoO_4 tetrahedra with near-ideal Mo^{VI}–O bond distances. Lithium and magnesium are distributed in the remaining three polyhedra, two of them octahedral [M(1) and M(2)] and the third trigonal prismatic [M(3)]. The distribution of lithium and magnesium obtained from the site occupancies (Table 2) is as follows: ($Li_{0.341}Mg_{0.659}$) at M(1), ($Li_{0.529}Mg_{0.471}$) at M(2) and ($Li_{0.790}Mg_{0.210}$) at M(3). Similar distributions of lithium and divalent metals have been reported for $Li_2Co_2(MoO_4)_3$[13] and $Li_2Ni_2(MoO_4)_3$.[11]

Our investigation of the Li_2O–MgO–MoO_3 system has shown that the framework structure (Fig. 1) is stable over a range of composition, represented by the formula $Li_{2-2x}Mg_{2+x}(MoO_4)_3$ for $0 \leqslant x \leqslant 0.3$ (Fig. 2). Lattice parameters and synthesis conditions for members of the $Li_{2-2x}Mg_{2+x}(MoO_4)_3$ series are given in Table 4. A similar range of solid solutions has also been reported for the Mn(II) system $Li_{2-2x}Mn_{2+x}(MoO_4)_3$, where an increase of x results essentially in a decrease of lithium content at the trigonal

Table 2 Positional and displacement parameters for $Li_2Mg_2(MoO_4)_3$

Atom	Wyckoff position	Occupancy	*x*/*a*	*y*/*b*	*z*/*c*	U_{eq}[a] or U_{iso}*/Å^2
Mo(1)	4c	1.0	0.22044(7)	1/4	0.05688(2)	0.00721(7)
Mo(2)	8d	1.0	0.27554(5)	0.02686(2)	0.84338(1)	0.00811(5)
Mg(1)	8d	0.659(2)	0.7529(3)	0.0750(1)	0.97230(6)	0.0099(3)*
Li(1)		0.341(2)				
Mg(2)	4c	0.471(5)	0.3984(5)	1/4	0.2492(1)	0.0153(6)*
Li(2)		0.529(5)				
Mg(3)	4c	0.210(4)	0.7433(7)	1/4	0.8013(2)	0.0123(9)*
Li(3)		0.790(4)				
O(1)	8d	1.0	0.5578(4)	0.1130(2)	0.8729(1)	0.0120(5)
O(2)	4c	1.0	0.1445(5)	1/4	0.1534(1)	0.0108(6)
O(3)	8d	1.0	0.4175(4)	0.1159(2)	0.0364(1)	0.0105(5)
O(4)	4c	1.0	0.9428(5)	1/4	0.9948(1)	0.0109(7)
O(5)	8d	1.0	0.3510(4)	0.8836(2)	0.7950(1)	0.0106(4)
O(6)	8d	1.0	0.0813(4)	0.9905(2)	0.9247(1)	0.0116(5)
O(7)	8d	1.0	0.0772(4)	0.1242(2)	0.7868(1)	0.0145(5)

[a] U_{eq} is defined as one-third of the trace of the orthogonalized $\mathbf{U}_{ij}$ tensor.

Table 3 Distances (Å) and bond valences (v. u.)

(a) concerning Mo atoms			
Mo(1)–O(2)	1.745(2)	1.549	
Mo(1)–O(3) × 2	2 × 1.765(2)	2 × 1.468	
Mo(1)–O(4)	1.793(3)	1.361	
		Σ = 5.846	
Mo(2)–O(1)	1.780(2)	1.410	
Mo(2)–O(5)	1.768(2)	1.456	
Mo(2)–O(6)	1.786(2)	1.387	
Mo(2)–O(7)	1.749(2)	1.533	
		Σ = 5.786	
(b) concerning atoms M(*n*) = Mg(*n*) − Li(*n*)			
M(1)–O(1)	2.055(2)	0.376(Mg)	0.204(Li)
M(1)–O(3)	2.099(3)	0.334(Mg)	0.181(Li)
M(1)–O(3)	2.186(2)	0.264(Mg)	0.143(Li)
M(1)–O(4)	2.110(2)	0.324(Mg)	0.175(Li)
M(1)–O(6)	2.076(2)	0.355(Mg)	0.192(Li)
M(1)–O(7)	2.117(2)	0.318(Mg)	0.172(Li)
		Σ = 1.971	1.067
M(2)–O(2) × 2	2.129(4)	2 × 0.308(Mg)	2 × 0.167(Li)
M(2)–O(5) × 2	2.050(3)	2 × 0.381(Mg)	2 × 0.206(Li)
M(2)–O(5) × 2	2.058(3)	2 × 0.373(Mg)	2 × 0.202(Li)
		Σ = 2.124	1.15
M(3)–O(1) × 2	2.133(3)	2 × 0.304(Mg)	2 × 0.165(Li)
M(3)–O(7) × 2	2.172(4)	2 × 0.274(Mg)	2 × 0.148(Li)
M(3)–O(7) × 2	2.206(3)	2 × 0.250(Mg)	2 × 0.135(Li)
		Σ = 1.656	0.896

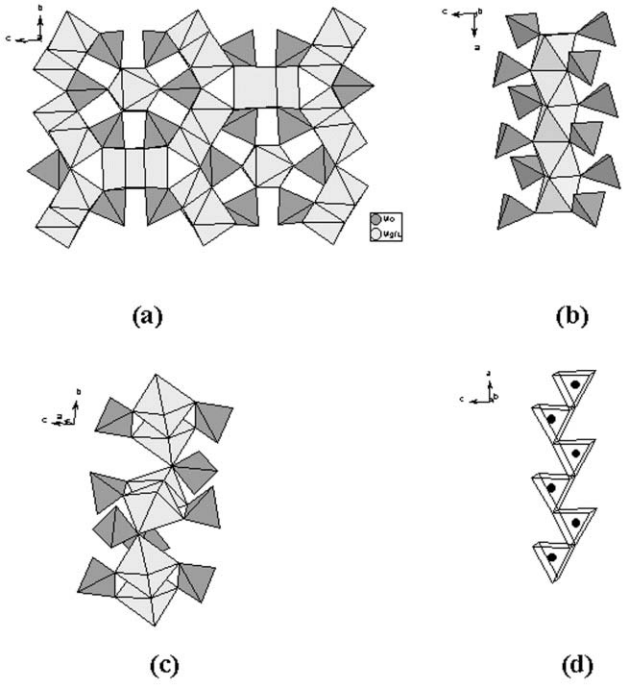

Fig. 1 Crystal structure of $Li_2Mg_2(MoO_4)_3$ showing (a) a view of the (100) plane, (b) the connectivity of M(1) octahedra, (c) the connectivity of M(2) octahedra and (d) the connectivity of M(3) trigonal prisms.

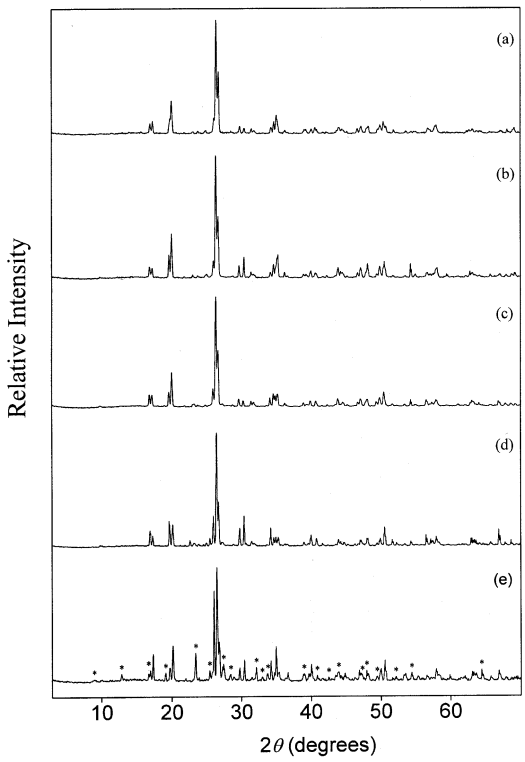

Fig. 2 Powder XRD patterns of $Li_{2-2x}Mg_{2+x}(MoO_4)_3$: (a) $x = 0$, (b) $x = 0.1$, (c) $x = 0.2$, (d) $x = 0.3$, (e) $x = 0.5$. In (e) the impurity reflections due to $MgMoO_4$ are marked by asterisks.

prismatic M(3) site,[12] besides creating cation vacancies at M(2) site.

^{7}Li NMR spectra of $Li_{2-2x}Mg_{2+x}(MoO_4)_3$ ($x = 0$ and 0.3) compounds were recorded. They both exhibit a central line and spinning side bands due to the first order quadrupolar interaction (Fig. 3). However, a close inspection of the central line shows that it is not symmetrical. The order of magnitude of the quadrupolar interaction can be evaluated by the first order spinning sideband. It leads to NuQ in the range of 30 to 50 kHz and precludes that the line shape of the central line can be due to the second order quadrupolar interaction effect. Therefore, the line shape must be related to several sites.

Several attempts with two components did not provide satisfactory agreement. A three component analysis provides an extremely good description of the central line shape (Fig. 3a and b). In addition, the first order quadrupolar pattern is also generated and spinning side bands are also quite well described with this approximation. However, due to an inherent

Table 4 Chemical composition, synthesis conditions and lattice parameters for $Li_{2-2x}Mg_{2+x}(MoO_4)_3$ and $Li_3M(MoO_4)_3$ (M = Cr, Fe)

Composition	Synthesis conditions/°C, h	Lattice parameters/Å			
		a	*b*	*c*	*V*/Å^3
$Li_2Mg_2(MoO_4)_3$	450,12; 575,12	5.1167(2)	10.4646(4)	17.6228(8)	943.58(7)
$Li_{1.8}Mg_{2.1}(MoO_4)_3$	450,12; 575,12	5.1038(2)	10.4865(5)	17.6632(7)	945.35(7)
$Li_{1.6}Mg_{2.2}(MoO_4)_3$	600,12; 600,6	5.0927(3)	10.5008(6)	17.689(1)	945.94(9)
$Li_{1.4}Mg_{2.3}(MoO_4)_3$	600,12; 600,12	5.0821(3)	10.5083(5)	17.6996(9)	945.24(9)
$Li_3Cr(MoO4)_3$	350,24; 600,24	5.0377(4)	10.4091(1)	17.6149(4)	923.71(9)
$Li_3Fe(MoO_4)_3$	550,12; 600,6	5.0697(3)	10.4333(5)	17.6317(9)	932.64(7)

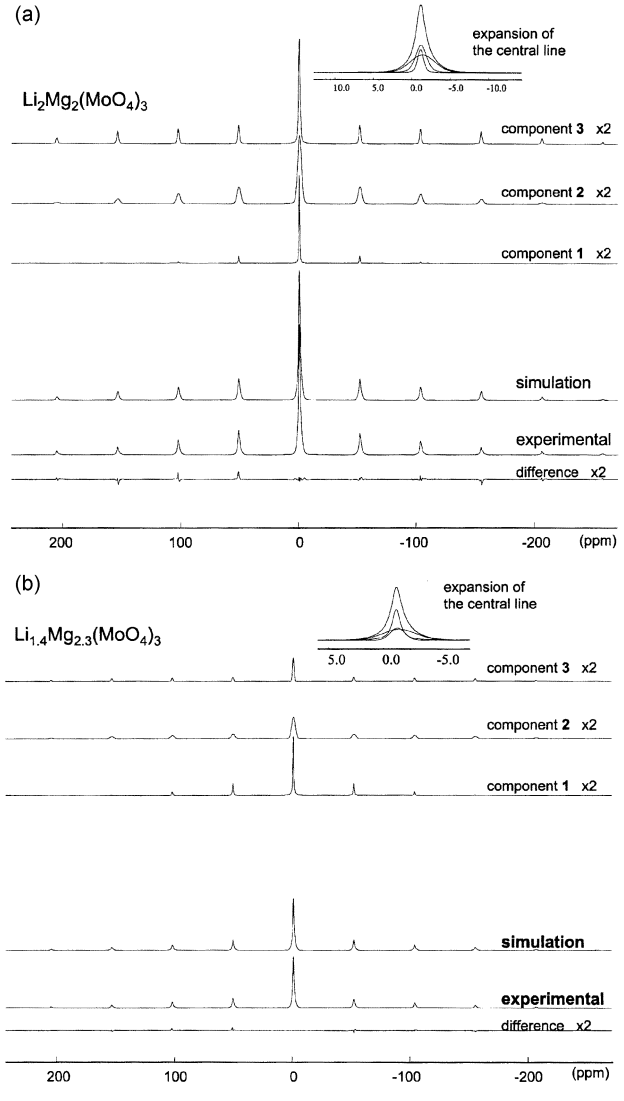

Fig. 3 Experimental, deconvoluted and simulated ^{7}Li NMR spectra of (a) $Li_2Mg_2(MoO_4)_3$ and (b) $Li_{1.4}Mg_{2.3}(MoO_4)_3$.

inaccuracy in the evaluation of individual line intensities, site fractions are rather different from those inferred from the X-ray structure analysis for $x = 0$ (Table 5a). This latter study indicates that Li atoms are distributed on three sites, M(1) (8d: 2.73 Li), M(2) (4c: 2.11 Li) and M(3) (4c: 3.16 Li). The corresponding values found by NMR are 0.86, 3.12 and 4.02 for $x = 0$, and 1.20, 2.01 and 2.39 for $x = 0.3$ (Table 5b). To fully assign the NMR lines to crystallographic sites with such fractional occupancies is difficult. Doing it on a rigorous basis would require both diffraction and NMR analyses of samples with different lithium contents. The main trends of site occupancies would change in a correlated way that would prove definitely the assignment.

At this stage of the investigation, only a tentative assignment can be provided, which also takes into account the following facts:

—if $Li_{2-2x}Mg_{2+x}(MoO_4)_3$ compounds behave as their Mn(II) analogs, which is likely, an increase of x would result in a decrease of Li content at the M(3) site;

—as suggested below, the conductivity is likely restricted to Li-ion in the M(3) sites.

Considering that both the line width and the quadrupolar interaction strongly depend on the site symmetry, we can suggest that component 1, with the smallest set of line width, NuQ and Li content, corresponds to the M(2) 4c site located on a mirror plane. With the largest NuQ value, component 3 could be assigned to M(1), an 8d site with the lowest symmetry. Therefore, component 2 would correspond to the M(3) site, in fair agreement with its Li content which is the largest for $x = 0$ and shows the most important decrease when x increases. The much larger line width of component 2 with respect to components 1 and 3 could be a consequence of the higher mobility of Li-ions in the M(3) sites. As a matter of fact, if the jump frequency of Li^+ is of the same order of magnitude as the Larmor frequency, a significant line broadening is expected.

We investigated the lithium ion conductivity of $Li_{2-2x}Mg_{2+x}(MoO_4)_3$ by a.c. impedance spectroscopy. The data (Fig. 4 and Table 6) show that the conductivity decreases with increasing x in the series $Li_{2-2x}Mg_{2+x}(MoO_4)_3$. Since an increase of x would be accommodated essentially by an increase of divalent metal content at the trigonal prismatic [M(3)] site,[12] we came to the natural conclusion that the occupancy at this site mainly governs the lithium ion conductivity: the higher the lithium ion content at the M(3) site, the higher the ionic conductivity. The curved Arrhenius plots (Fig. 4) however suggest a competing conduction mechanism, possibly arising from lithiums occupying more than one site.

An examination of the framework structure (Fig. 1) for possible pathways for lithium ion migration reveals that although the framework is three-dimensional, lithium ion mobility would be restricted mainly to the one-dimensional channels formed by alternating cation-occupied and vacant trigonal prisms [M(3) site] (Fig. 1d). One could visualize migration of lithium from an occupied trigonal prism to the neighboring vacant prism through the rectangular windows that are common between them. Dimensions of the rectangular window ($\sim$3.95 $\times$ $\sim$ 4.00 Å) would easily permit such a migration of lithium. A similar pathway does not exist for the migration of lithium ions at the octahedral M(1) and M(2) sites.

Having rationalized that lithium ion conduction in these materials is most likely restricted to trigonal prismatic chains along the *a* direction (Fig. 1d), we expected that the presence of divalent cations at this site would impede the motion of lithium and therefore decrease the lithium ion conductivity. Accordingly, a decrease of ionic conductivity with increasing x in the series, $Li_{2-2x}Mg_{2+x}(MoO_4)_3$ is consistent with an increase in the Mg(II) content at M(3) sites for $x > 0$. As a corollary, we expected that a material where the M(3) sites are occupied only by lithium would exhibit a higher lithium ion conductivity than $Li_{2-2x}Mg_{2+x}(MoO_4)_3$. Molybdates of the formula

Table 5 Results of spectral decomposition of ^{7}Li NMR spectra[a]

(a) for $Li_2Mg_2(MoO_4)_3$

Li/site	Li fraction (%)	Chemical shift (ppm)	Line width (ppm)	G/L[b]	NuQ/kHz	ηQ	Component no.
3.12/M(1)	39.0	−1.20	1.71	0.61	45	1.0	3
0.86/M(2)	10.7	−1.14	0.95	0.62	15	1.0	1
4.02/M(3)	50.3	−1.20	3.82	0.87	35	1.0	2

(b) for $Li_{1.4}Mg_{2.3}(MoO_4)_3$

Li/site	Li fraction (%)	Chemical shift (ppm)	Line width (ppm)	G/L[b]	NuQ/kHz	ηQ	Component no.
2.01/M(1)	35.8	−1.30	1.59	0.61	45	1.0	3
1.20/M(2)	21.5	−1.20	0.80	0.62	25	1.0	1
2.39/M(3)	42.7	−1.46	3.65	0.87	40	1.0	2

[a]Note: estimated uncertainty is 10–15%. [b]G/L is the proportion of Gaussian to Lorentzian components in the line shape. G/L = x × Gaussian/(1 − x) × Lorentzian. When x = 0, the line shape is pure Lorentzian and *vice versa*.

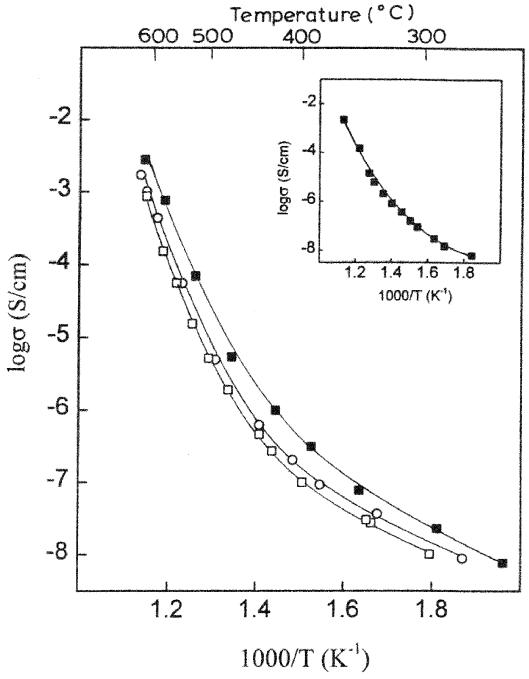

Fig. 4 Arrhenius plots for lithium ion conductivity of $Li_{2-2x}Mg_{2+x}(MoO_4)_3$ for x = 0 (■), x = 0.1 (O), and x = 0.3 (□). The corresponding data for the x = 0.2 member are shown in the inset. The solid lines connecting the data points are a guide to the eye.

Table 6 Lithium ion conductivity data for $Li_{2-2x}Mg_{2+x}(MoO_4)_3$ and $Li_3M(MoO_4)_3$ (M = Cr, Fe)

Composition	$\sigma_{300\ °C}$/S cm^{-1}	$\sigma_{600\ °C}$/S cm^{-1}	E_a (±0.02)/eV
$Li_2Mg_2(MoO_4)_3$	1.1×10^{-7}	2.7×10^{-3}	0.71 (200–400 °C)
			2.32 (400–600 °C)
$Li_{1.8}Mg_{2.1}(MoO_4)_3$	6.1×10^{-8}	1.7×10^{-3}	0.63 (200–400 °C)
			2.19 (400–600 °C)
$Li_{1.6}Mg_{2.2}(MoO_4)_3$	1.4×10^{-8}	9.3×10^{-4}	0.76 (190–400 °C)
			2.06 (400–600 °C)
$Li_{1.4}Mg_{2.3}(MoO_4)_3$	1.0×10^{-8}	8.7×10^{-4}	0.62 (280–400 °C)
			2.34 (400–600 °C)
$Li_3Cr(MoO_4)_3$	2.6×10^{-6}	3.9×10^{-3}	1.06 (200–600 °C)
$Li_3Fe(MoO_4)_3$	6.6×10^{-7}	1.4×10^{-3}	1.11 (200–600 °C)

$Li_3M^{III}(MoO_4)_3$ for M^{III} = Cr and Fe, which are isotypic with $Li_2M_2^{II}(MoO_4)_3$, are known in the literature.[10,22] It appears that in these materials, the trigonal prismatic sites are exclusively occupied by lithium.[10] Accordingly, we investigated the lithium ion conductivity of $Li_2M^{III}(MoO_4)_3$ oxides and the results (Fig. 5 and Table 6) show that indeed these materials exhibit a higher conductivity than that of $Li_{2-2x}Mg_{2+x}(MoO_4)_3$, lending support to the idea that these molybdates are 'one-dimensional' lithium ion conductors where the conductivity appears to be restricted to the motion of lithium in the trigonal prismatic channels along the a axis. Significantly, the conductivities of $Li_3M(MoO_4)_3$ oxides are comparable to or even better than the conductivity of well-known one-dimensional lithium ion conductors such as $LiAlSiO_4$[23] and $LiSbO_3$.[24] Further work using single crystals is essential to establish the one-dimensional nature of ionic conductivity in $Li_3M(MoO_4)_3$ and $Li_{2-2x}Mg_{2+x}(MoO_4)_3$ materials.

Conclusion

Lithium magnesium molybdates of the formula $Li_{2-2x}Mg_{2+x}(MoO_4)_3$ ($0 \leqslant x \leqslant 0.3$), possessing a novel framework consisting of interconnected octahedra, trigonal prisms and MoO_4 tetrahedra, have been investigated for lithium ion conduction. The crystal structure of one of the members, $Li_2Mg_2(MoO_4)_3$, has been determined from single crystals using X-ray diffraction and the distribution of lithium at the

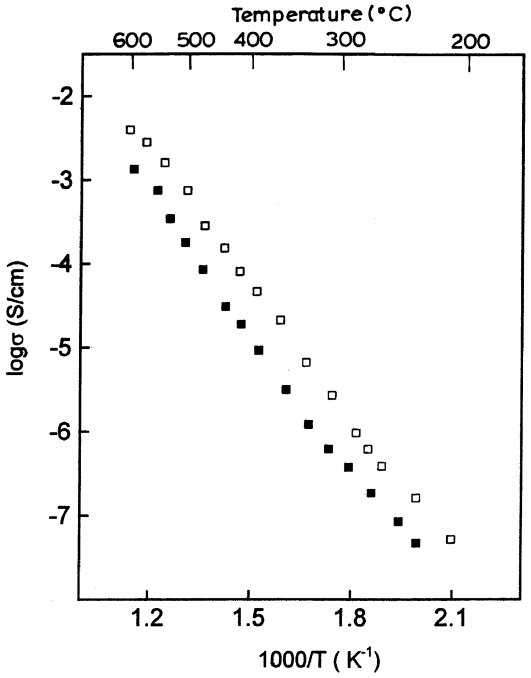

Fig. 5 Arrhenius plots for lithium ion conductivity of $Li_3Cr(MoO_4)_3$ (□) and $Li_3Fe(MoO_4)_3$ (■).

octahedral and trigonal prismatic sites has been estimated for two compositions ($x = 0$ and $x = 0.3$) from ^{7}Li NMR spectral data. The results suggest that lithium ion conductivity is likely restricted to the one-dimensional channels of trigonal prisms which run parallel to the *a* axis. A higher conductivity of isotypic $Li_3M^{III}(MoO_4)_3$ (M = Cr, Fe) where trigonal prismatic sites are occupied exclusively by lithium lends support to this conclusion.

Acknowledgements

We thank the Council of Scientific and Industrial Research, New Delhi and the Department of Science and Technology, Government of India, for support of this research. Thanks are also due to Dr Gerhard Fink, Université Louis Pasteur, Strasbourg, France, for collection of NMR data.

References

1 J.-M. Tarascon and M. Armand, *Nature*, 2001, **414**, 359.
2 Guest editors D. R. Sadoway and A. M. Mayes, *MRS Bull.*, 2002, **27**(8), (whole issue).
3 D. Guyomard, in *New Trends in Electrochemical Technology: Energy Storage Systems in Electronics*, ed. T. Osaka and M. Datta, Gordon and Breach Publishers, Philadelphia, 2000, ch. 9.
4 A. D. Robertson, A. R. West and A. D. Ritchie, *Solid State Ionics*, 1997, **104**, 1.
5 H. Y. P. Hong, *Mater. Res. Bull.*, 1976, **11**, 73.
6 H. Aono, N. Imanaka and G.-Y. Adachi, *Acc. Chem. Res.*, 1994, **27**, 265.
7 V. Thangadurai, A. K. Shukla and J. Gopalakrishnan, *J. Mater. Chem.*, 1999, **9**, 739.
8 B. L. Cushing and J. B. Goodenough, *J. Solid State Chem.*, 2001, **162**, 176.
9 L. Sebastian, J. Gopalakrishnan and Y. Piffard, *J. Mater. Chem.*, 2002, **12**, 374.
10 R. F. Klevtsova and S. A. Magarill, *Sov. Phys. Crystallogr.*, 1971, **15**, 611.
11 M. Ozima, S. Sato and T. Zoltai, *Acta Crystallogr., Sect. B*, 1977, **33**, 2175.
12 S. F. Solodovnikov, Z. A. Solodovnikova, R. F. Klevtsova, L. A. Glinskaya, P. V. Klevtsov and E. S. Zolotova, *J. Struct. Chem.*, 1994, **35**, 871.
13 M. Wiesmann, I. Svoboda, H. Weitzel and H. Fuess, *Z. Kristallogr.*, 1996, **210**, 525.
14 T. Roisnel and J. Rodriguez-Carjaval, *Physica B*, 1993, **192**, 55.
15 G. M. Sheldrick, SHELXTL PLUS 5.0, Siemens Analytical X-Ray Instruments Inc., Madison, WI, 1990.
16 V. Petricek and M. Dusek, JANA98, Institute of Physics, Academy of Sciences of the Czech Republic, Prague, Czech Republic, 1998.
17 D. T. Cromer and J. T. Waber, in *International Tables for X-Ray Crystallography*, vol. IV, Tables 2.2B and 2.3.1, Kynoch Press, Birmingham, England, 1974.
18 D. Massiot, F. Fayon, M. Capron, I. King, S. Le Calvé, B. Alonso, J.-O. Durand, B. Bujoli, Z. Gan and G. Hoatson, *Magn. Reson. Chem.*, 2002, **40**, 70.
19 N. E. Brese and M. O'Keeffe, *Acta Crystallogr., Sect. B*, 1991, **47**, 192.
20 I. D. Brown and D. Altermatt, *Acta Crystallogr., Sect. B*, 1985, **41**, 244.
21 W. Kraus and G. Nolze, POWDERCELL, a Program for the Representation and Manipulation of Crystal Structures and Calculation of the Resulting X-ray Powder Patterns, *J. Appl. Crystallogr.*, 1996, **29**, 301.
22 V. L. Butukhanov, E. I. Get'man and M. V. Mokhosoev, *Russ. J. Inorg. Chem.*, 1972, **17**(4), 609.
23 U. V. Alpen, E. Schonherr, H. Schultz and G. H. Talat, *Electrochim. Acta*, 1977, **22**, 805.
24 K. Ozawa, Y. Sakka and M. Amani, *Mater. Res. Soc. Symp. Proc.*, 1997, **453**, 617.